DOI 10.24425/aee.2024.150883

Influence of the radiofrequency applicators arrangement on the sizes of ablative zones inside hepatic tumor

Piotr Gas [1], **Arkadiusz Miaskowski** [2]✉

[1] *Department of Electrical and Power Engineering*
AGH University of Krakow
30 Mickiewicza Ave., 30-059 Krakow, Poland

[2] *Lublin University of Technology*
Faculty of Electrical Engineering and Computer Science
38A Nadbystrzycka Str., 20-618 Lublin, Poland

e-mail: piotr.gas@agh.edu.pl, ✉ *a.miaskowski@pollub.pl*

(Received: 15.10.2023, revised: 22.08.2024)

Abstract: Radiofrequency (RF) ablation is a popular therapeutic technique for heating solid tumors that are medically unsuitable for resection or other treatments. Thermal ablation applicators create high-frequency electromagnetic fields (EMFs) within the tumor site, which causes heating, coagulation, and ultimately death of the cancer cells. The aim of this study is the numerical analysis of the temperature distributions, ablation zones, and specific absorption rates (SAR) during RF ablation in relation to an ellipsoidal shaped tumor placed in the model of liver tissue. The source of heat is a three-element system of RF needle applicators operating at a frequency 100 kHz, with a given electrode potential, inserted into the tumor. In order to obtain an appropriate temperature distribution in the target area, the Laplace equation coupled with the Pennes equation were solved using the finite element method (FEM). The arrangement effect of three needle-type applicators on the resultant thermal profiles and the volumes of ablation zones were analyzed and compared. In addition, the ablation zones for various angles of the RF applicator placed in the center of the tumor were analyzed. The paper shows that in order to control temperature distribution and ablation zones the proposed system of RF applicators and the arrangement of electrodes can be successfully applied in hepatocellular carcinoma treatment.

Key words: ablation zones, computational modeling, finite element method, heating techniques, hepatocellular carcinoma, percutaneous thermal ablation, RF electrodes

1. Introduction

Hepatocellular carcinoma stands as the prevailing malignant tumor affecting the human liver of expanding part of the general population [1,2]. In the majority of instances, hepatic malignancies cannot be eradicated by a simple surgical resection. This is principally attributed to the large tumor dimensions and complex structure of multifocal liver tumors, their specific placement, and densely vasculared blood network. Hence, the pursuit for novel and less invasive methods of generating therapeutic heat within the cancer, thereby sparing healthy liver tissue while focusing heat exclusively into the targeted tumor volume, remains a pressing endeavor [3, 4]. Examples of these heat focused therapies are referred to as interstitial hyperthermia and thermal ablation procedures [5–7], both of which harness radiofrequency (RF) energy [8, 9] or microwaves [10, 11] to destroy cancerous cells. The interstitial needle-like applicators, owing to their straightforward construction [12, 13], obviate the necessity for laparotomy and can be administered percutaneously under general anesthesia [14]. The typical instruments employed for thermotherapy can be regulated based on temperature or EM power changes [4]. In addition, the positions of temperature sensors may be controlled by image-guided techniques during the whole treatment [15]. Tissue temperatures during the ablation process may escalate to substantial levels, ranging from 50°C to 100°C and even more [4], and when coupled with precise timing, may ultimately culminate in coagulation and necrosis of cancerous tissue [16–18]. It is worth noting that the thermal damage of hepatic tumors transpires with a specific margin of ablative tissue necrosis, challenging its unequivocal identification through existing imaging modalities during ablation treatments. This presents the potential for thermal harm to adjacent nerves, blood vessels, and adjacent tissues, thus constraining the utility of this treatment method [19]. Additionally, the unsuitable structure of employed applicators, their placements, and the applied power deposition can contribute to incomplete destruction of cancerous cells and foster the resurgence of neoplastic disease.

In the literature, new technological solutions are being sought to obtain conformal ablation adapted to the type and shape of the tumor, as well as the dielectric properties of the cancerous tissue and its surroundings. For this purpose, researchers design various types of applicators operating at radio (RF ablation) and microwave (MW ablation) frequencies. The thermal ablation applicators used take the shape of a needle [3, 15] or more complex multi-tines structures [4, 16]. In most cases, the applicator design process involves selecting the optimal antenna sizes to obtain the best possible impedance matching of the applicator to the tissue, which is reflected in the lowest value of reflection coefficient/return loss (S_{11}) [20]. Kernot *et al*. [21] compared the four most popular probe concepts used in ablation therapies: monopoles, single-slot, dual-slot, sleeve needle applicators, and showed that the most sensitive to tissue dielectric changes is the sleeve antenna, which has almost circular shape of temperature and specific absorption rate (SAR) patterns. Multi-slot coaxial antennas [6, 20], having additional air gaps in their structure, are characterized by more oval shapes of the ablation zones, and increasing the number of coaxial slots increases the therapeutic range and the possibility of treating tumors of extended sizes. As shown by Xu *et al*. [22], adding π-matching networking in the multi-slot coaxial antenna structure, creates near-spherical ablation zones and minimizes thermal damage of healthy tissues surrounding the tumor [7]. It is also possible to optimize the antenna structure to obtain optimal shapes of ablation zones without analyzing the S_{11}-distribution [10]. Satish and Repaka [16] proposed a novel L shaped dual-frequency trocar with two tines: flexible curved one and static longitudinal one.

The authors noticed that irregular ablation areas could be obtained for the applicator in which individual tines were supplied by two different frequencies (2.45 GHz and 6 GHz) at the same time. The observed sizes of ablation zones were larger than when using a single frequency of 2.45 GHz. However, when a higher frequency was used (6 GHz), more spherical shapes of tumor tissue damage with a diameter up to 3 cm were found. Larger tumors, with a diameter above 5 cm, should be treated using applicators combined in the array of two or more probes [18]. Avishek *et al*. [23] investigated the influence of materials properties of Ni–Ti, Pt–Ir, Au, and Cu electrodes employed in hepatic RF ablation. However, they observed a marginal difference both in maximum temperatures and in ablation volumes.

During the process of designing therapeutic probes, researchers take steps to minimize the level of backward heating at the antenna-tissue interface, which occurs by using a cooling system for the internal structure of the applicator (water-cooled antennas) [10] or adding various chokes in choke and cap-choke antennas [7]. Enhancing the therapeutic effect and shortening the treatment time can be achieved by additionally placing magnetic nanoparticles (MNPs) in the treated tissue [8, 12, 24]. As shown by Tang *et al*. [25], the use of a multi-criterion Nelder–Mead optimization in magnetic hyperthermia treatment allows obtaining the optimal value of power dissipated in the MNP-saturated tissue and better convergence rate of performed simulation. Singla *et al*. [12] showed that the usage of the Nelder–Mead optimization works effectively in the case of magnetic fluids heated by various needle applicators (monopoles, dipoles, coaxial-slot, tapered-slot), but the lowest values of the S_{11}-coefficient they recorded for the tapered-slot antenna in the presence of gold coated iron based magnetite MNPs (Au@Fe_3O_4) with 20 nm magnetic core. Other similar investigations are expounded in some papers [26–41].

Based on the papers [3,4], the authors created a 3D model of three partially insulated RF probes immersed inside a liver phantom tissue including hepatic tumor. The ellipsoid shape of liver tumor was selected on the basis of previous authors' investigation [3], as the optimal one corresponding to the irregular shape of anatomical tumor. In this paper, the effect of the arrangement of three voltage-supplied applicators on the resultant thermal profiles of the hepatic tumor and the shapes of the result ablative zones were compared. In addition, the ablation zones for different rotation angles of the RF applicator placed in the center of the hepatic tumor were analyzed, which is a new authors' contribution in the subject.

2. Basic equations governing the model

The anatomical model of liver tissue including the partially isolated probe and ellipsoid tumor is shown in Figs. 1–2. In order to shorten the calculation time, the computational area was limited to a cube with a side of 115 mm as depicted in Fig. 2. The RF applicator of 50 mm length was inserted in the z-direction into the liver phantom. The electric potential of $\varphi = 25$ V was assumed on the lower electrode (no. 2), whereas the upper electrode (no. 1) was grounded ($\varphi = 0$). The upper dielectric (no. 1) with a length of 38.5 mm and a diameter of 0.5 mm was surrounded by a plastic catheter measuring 37 mm in length and 0.7 mm in diameter, which served as a protective element. All dimensions of the employed RF electric probe were adopted from [3] and listed in Table 1.

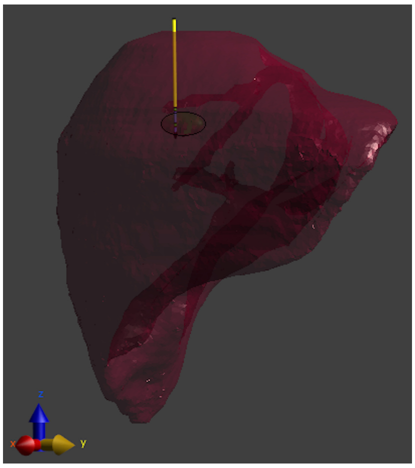

Fig. 1. Model of the hepatic tissue including ellipsoidal tumor and RF applicator

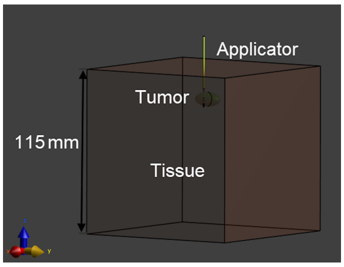

(a)

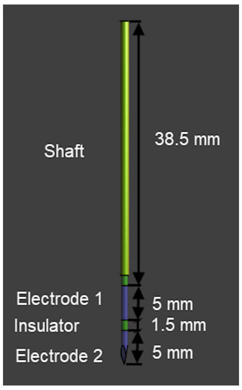

(b)

Fig. 2. Considered computational model of the:
(a) liver and tumor tissues, and (b) RF applicator employed in thermal ablation procedure

Table 1. Geometrical dimensions of the RF applicator

Applicator Elements	**Size** (mm)
radius of the shaft (trocar)	0.7
radius of the insulator	0.5
radius of the electrodes	0.5
length of the shaft	38.5
length of the insulator	1.5
length of the electrodes	5.0

In the analyzed 3D electro-conductive model, for simplicity, a quasi-static approximation was assumed and therefore the following equations could be used [3]:

$$\nabla \cdot \boldsymbol{J} = 0, \tag{1}$$

$$\boldsymbol{J} = \sigma \boldsymbol{E}, \tag{2}$$

$$\boldsymbol{E} = -\nabla \varphi, \tag{3}$$

where: $\boldsymbol{J}$ (A/m^3) and $\boldsymbol{E}$ (V/m) mean the vectors of current density and electric field strength, σ (S/m) corresponds to the electric conductivity of a medium and φ (V) stands for the electric potential supplied the RF electrodes.

In current model a quasi-static approximation is valid since for frequency of 100 kHz, the wavelength in vacuum ($\lambda_0 = c_0/f \approx 3$ km) and inside the liver tissue ($\lambda_{\text{eff}} = \lambda_0/\sqrt{(\varepsilon_r')} = 34.617$ m), where ε_r' is the tissue permittivity) [20] are many times larger than the largest dimension of RF applicator (see Table 1). Consequently, displacement currents are many times lower than conduction currents and can be negligible [3]. Additionally, in the computer simulation of all the modeled tissues are assumed as isotropic, homogeneous and linear media with constant parameters. Since the electric potential voltaged RF electrodes generate the electric field inside computational domain, the generalized Laplace equation is used to solve the problem [4, 23]:

$$\nabla \cdot (-\sigma \nabla \varphi) = 0. \tag{4}$$

On the other hand, the temperature field distribution inside biological objects under RF heating can be computed using the Pennes bioheat transfer equation [42]:

$$\rho C \frac{\partial T}{\partial t} + \nabla \cdot (-\kappa \nabla T) = \rho_b C_b \omega_b (T_b - T) + Q_{\text{ext}} + Q_{\text{met}}, \tag{5}$$

where ρ, C, and κ correspond to the density (kg/m^3), specific heat (J/(kg·K)), and thermal conductivity of a given medium (W/(m·K)), respectively, T means the tissue temperature (K), and t is the treatment time (s); the blood parameters are marked with a subscript 'b'and the blood perfusion rate inside biological tissues is denoted as ω_b (1/s). Moreover, the penultimate term Q_{ext} (W/m^3) stands for the volumetric power density due to the Joule heating produced by the RF needle-type applicators, namely [4, 11, 29]:

$$Q_{\text{ext}} = \boldsymbol{J} \cdot \boldsymbol{E} = 0.5\sigma \left|\boldsymbol{E}\right|^2 = 0.5\sigma \left|\nabla\varphi\right|^2, \tag{6}$$

where $|\boldsymbol{E}|$ (V/m) stands for the maximum value of electric field intensity. On the other hand, Q_{ext} can be express in the terms of specific absorption rate SAR (W/kg) which measures the EM energy deposited in unit mass of tissue and can be given by [3, 43]:

$$\text{SAR} = \frac{\sigma}{2\rho} \left|\boldsymbol{E}\right|^2 = \frac{\sigma}{2\rho} \left|\nabla\varphi\right|^2. \tag{7}$$

The last term in Eq. (5), $Q_{\text{met}} = \rho$HGR (W/m^3) means the volumetric power density due to tissue cells metabolism, where HGR (W/kg) is the heat generation rate [3, 44]. The cooling effects of blood perfusion through the liver tissue are often expressed by the heat transfer rate HTR (mL/min/kg), namely $\omega_b = \alpha \cdot \rho$HTR (1/s), where α is the scaling factor [44].

To simulate the analyzed multphysics problem, the additional initial/boundary conditions for main Eqs. (4) and (5) are necessary. An electric potential has a zero value ($\varphi = 0$) at initial time. The Direchlet boundary conditions ($\varphi = 0$) were set at the external boundaries of 3D model and the electrode no. 1. The voltage of $\varphi = 25$ V was applied on the electrode no. 2 (Fig. 1). Moreover, the normal components of the current density vector were assumed as continuous at the internal boundaries of the considered model, namely [13, 23]:

$$\boldsymbol{n} \cdot (\boldsymbol{J}_1 - \boldsymbol{J}_2) = 0, \tag{8}$$

which, depending on the electric potential, takes the form as below [3]:

$$\boldsymbol{n} \cdot (\sigma_1 \nabla \varphi_1 - \sigma_2 \nabla \varphi_2) = 0. \tag{9}$$

The similar conditions should be defined for the temperature field. The initial temperature in whole model is equal to T_0. On the external boundaries of the model, thermal insulation ($\partial T / \partial n = 0$) was assumed. At the internal boundaries, the heat flow continuity was adopted according to the formula [23]:

$$\boldsymbol{n} \cdot (\kappa_1 \nabla T_1 - \kappa_2 \nabla T_2) = 0, \tag{10}$$

where $\boldsymbol{n}$ stands for the normal vector perpendicular to a given boundary. The subscripts 1 and 2 correspond to values of given quantity at two different sides of the same boundary.

3. Simulation results

The current model assumes a quasi-static approximation and is valid for a frequency of $f = 100$ kHz. The parameters used for modelling liver tissue, blood and an RF applicator have been taken from [3, 44] and listed in Table 2. The dielectric components of the RF applicator (dielectrics and plastic catheter) were modeled using polyethylene material with an electrical conductivity of $\sigma = 0.5$ mS/m and a mass density of $\rho = 1000$ kg/m^3. The electrodes were modeled as perfect electric conductor (PEC) materials. The initial tissue temperature was assumed as $T_0 = 37°$C and the blood temperature had constant value of $T_b = 37°$C. All FEM-based calculations are performed using the commercially available Sim4Life software [45].

Table 2. Electro-thermal parameters for 100 kHz employed in the analyzed model [3, 44]

Tissues	$\boldsymbol{\sigma}$ (mS/m)	$\boldsymbol{\rho}$ (kg/m^3)	$\boldsymbol{C}$ (J/(kg·K))	$\boldsymbol{\kappa}$ (W/(m·K))	**HGR** (W/kg)	$\boldsymbol{\rho_b C_b \omega_b}$ (kW/m^3/K)	$\boldsymbol{\omega_b}$ (1/s)
Blood	703.0	1050	3617	0.520	0	664.6	0.1750
Liver tissue	84.6	1079	3540	0.520	9.93	62.7	0.0165
Liver tumor	400	1040	3437	0.563	12.0	51.0	0.0134

In our case, three scenarios of placement of needle probes inside the hepatic tissue were analyzed: forming single- (probe no. 1), double (probes no. 1 and 2), and triple- (probes no. 1, 2, and 3) applicator systems for RF ablation, as shown in Fig. 3. All needle probes, placed 2 mm apart, were inserted into an ellipsoidal liver tumor along the shorter axis of the ellipse lying along the z-axis and the applicator no. 3 was located exactly in the center of the tumor. Such arrangement of the RF electrodes was intended to ignore the effect of tumor symmetry on the resulting temperature profiles of the cancer tissue. Additionally, the point P is marked in Fig. 3, where the transient temperature curves were observed.

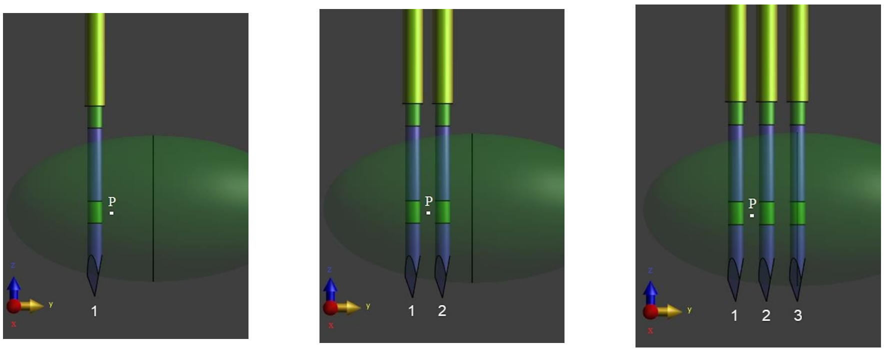

(a) (b) (c)

Fig. 3. Analized scenarios of arrangements of RF probes in the case of: (a) single-; (b) double-, and (c) triple-applicator system for RF ablation treatment

Figure 4 compares the spatial temperature distributions inside hepatic tumor tissue in the steady-state derived from all considered RF ablation systems. In all analyzed cases, the highest temperatures were observed in the vicinity of the insulator separating the two electrodes of each RF probe. As expected, with the number of active applicators, the therapeutic range of temperature operation extends along the y-axis, while changes in heat penetration in other directions are relatively small. This is also seen in the time-dependent heat profiles of the liver tumor shown in Fig. 5, measured in the observation point P = (0, −3, 0) mm located in middle height of insulator, in the middle distance separating two electrodes in the double-probe system (see Fig. 3(b)). After 10 min-ablation procedure, the tumor temperature reached a therapeutic level of 96°C for 3 employed probes and respectively 91°C and 80°C for 2 and 1 used probes.

Next Fig. 6 presents the SAR distributions inside liver tissues in the steady-state for three considered arrangements of the employed RF probes. The SAR values were presented in decibel scale compared to the maximum SAR level for better graphical illustration. In the following drawings, it can be seen that the SAR values are enhanced inside the tumor site, which results from the specific electrical properties of the malignant liver tissue and the geometry of the tumor.

From the medical point of view, isothermal (ISO) surfaces above 50°C can be considered as characteristic ablative zones. Figure 7 illustrates three sample ISO-surfaces (ISO-50, ISO-60 and ISO-75) in the yz-plane after 10 min treatment for temperatures levels of 50°C, 60°C, and 75°C, respectively. The conclusions are similar to those resulting from the temperature distributions shown in Fig. 4, however, this time the exact volumes of the ablation zones can be computed and compared with the volume of ellipsoidal hepatic tumor (V_{tumor} = 1047.46 mm^3), as gathered together in Table 3 for various active RF probes configurations. The performed calculations show

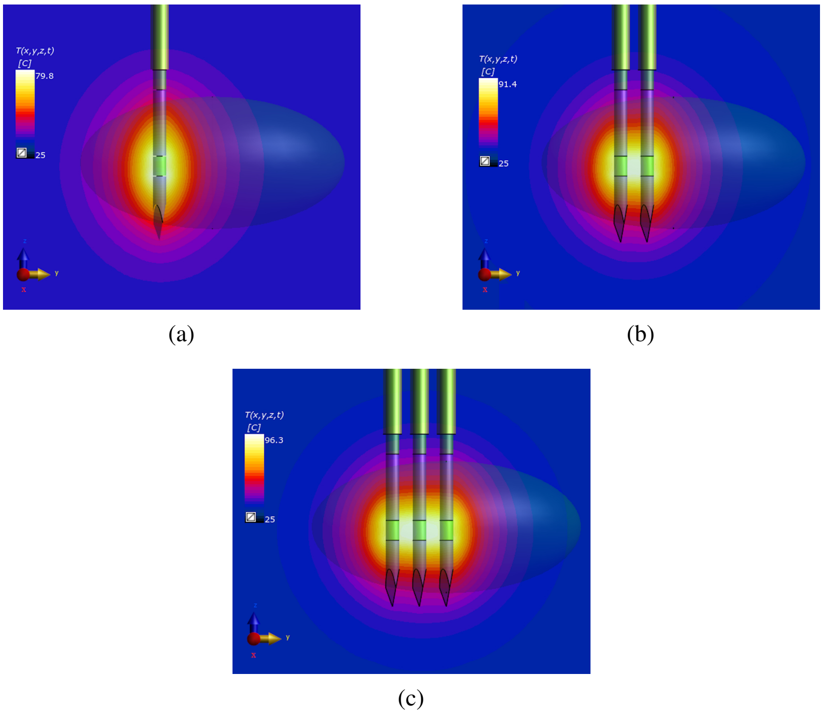

Fig. 4. Temperature distributions inside liver tumor tissue in the case of: (a) single-; (b) double-, and (c) triple-applicator system for RF ablation treatment in the steady-state

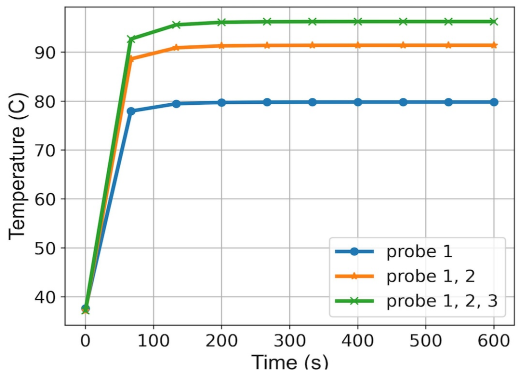

Fig. 5. Transient temperature distributions inside liver tumor tissue at the observation point P = (0, −3, 0) mm in the case of: (a) single-; (b) double-, and (c) triple-applicator system

that the ablation zones increase with the number of active applicators and in the best case of triple-probe RF ablation system, they are 71.5%, 18.9% and 5.5% of the tumor volume, respectively for ISO-50, ISO-60 and ISO-75 surfaces.

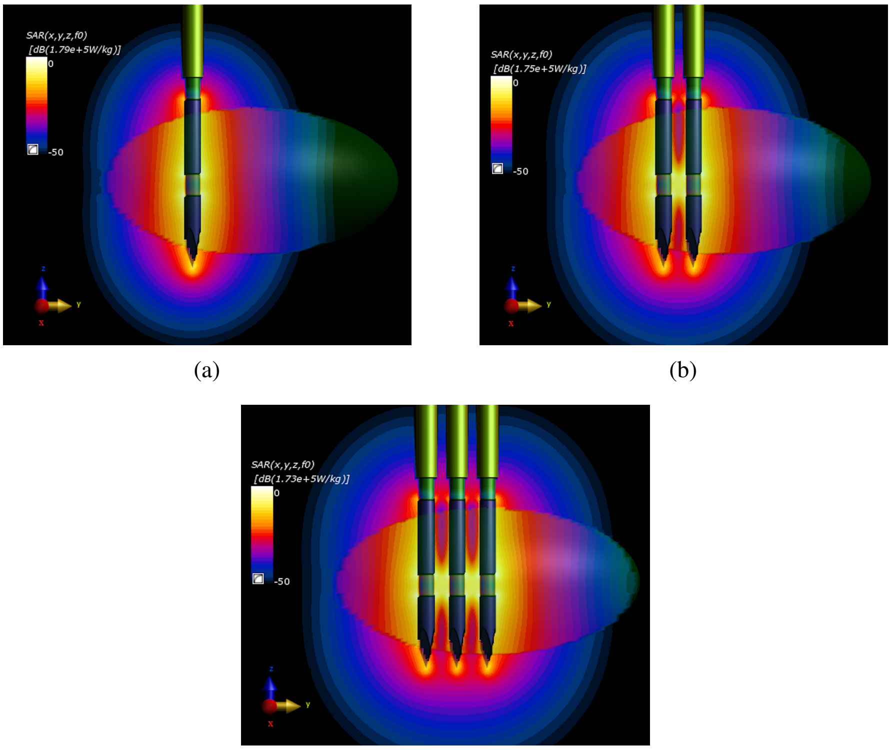

(a) (b)

(c)

Fig. 6. SAR distributions inside liver tumor tissue in the case of: (a) single-; (b) double-, and (c) triple-applicator system for RF ablation treatment in the steady-state

Table 3. Calculated ablation volumes for different isothermal (ISO) surfaces

Numbers of Active RF Probes	**Ablation Volumes**					
	$V_{\mathbf{ISO\text{-}50}}$ (mm^3)	$V_{\mathbf{ISO\text{-}50}}$ (%)	$V_{\mathbf{ISO\text{-}60}}$ (mm^3)	$V_{\mathbf{ISO\text{-}60}}$ (%)	$V_{\mathbf{ISO\text{-}75}}$ (mm^3)	$V_{\mathbf{ISO\text{-}75}}$ (%)
1	219.838	21.0	43.767	4.2	3.963	0.4
1, 2	473.837	45.2	116.145	11.1	25.243	2,4
1, 2, 3	749.455	71.5	197.634	18.9	53.382	5.1

Finally, the influence of rotation angles of the RF applicator on the resultant SAR values (Fig. 8) and ablation zones (Fig. 9) in the steady state were analyzed.

This time a needle applicator no. 3 was inserted into the center of the ellipsoidal hepatic tumor the angle ϕ that formed by the axis of the RF probe with the shorter axis of the tumor ellipse lying along the z-axis. The RF applicator rotation angle was changed from 0° to 90°. Figure 8 shows

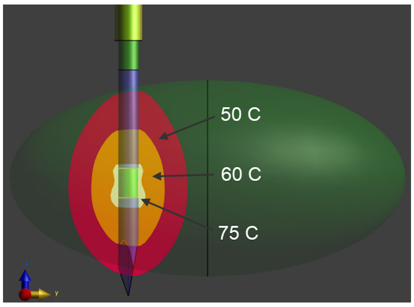

(a)

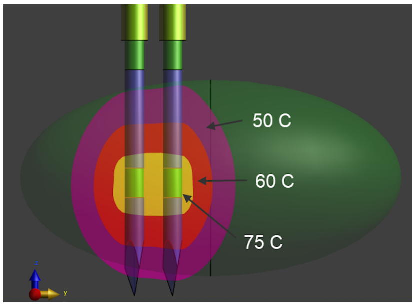

(b)

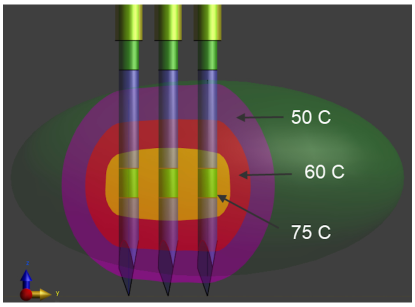

(c)

Fig. 7. The isothermal (ISO) surfaces inside liver tumor tissue for temperature 50°C, 60°C and 75°C in the case of: (a) single-; (b) double-, and (c) triple-applicator system in the steady state

that the rotation of the needle applicator, from the shorter axis to the longer axis of the tumor ellipse, causes the uniformity of SAR distributions, and the best match was obtained when the RF probe was inserted along the z-axis. At the same time, changing the position of the applicator does not cause significant changes in the size of the ablative zones (Fig. 9). Increasing the rotation angle of the applicator slightly increases ablation volumes from 17.7% to 19.5% of ellipsoid liver tumor volume as given in Table 4.

Table 4. Ablation volumes for ISO-50°C surface in the case of various RF applicator rotation angles

	RF Applicator Rotation Angles			
	$\phi = 0°$	$\phi = 30°$	$\phi = 60°$	$\phi = 90°$
RF Probe No. 3 (in the liver tumor centre)	**Ablation Volumes**			
	$V_{\text{ISO-50}}$ (mm^3)	$V_{\text{ISO-50}}$ (mm^3)	$V_{\text{ISO-60}}$ (mm^3)	$V_{\text{ISO-75}}$ (mm^3)
	185.806	188.887	201.133	203.648
	$V_{\text{ISO-50}}$ (%)	$V_{\text{ISO-50}}$ (%)	$V_{\text{ISO-50}}$ (%)	$V_{\text{ISO-50}}$ (%)
	17.7	18.0	19.2	19.4

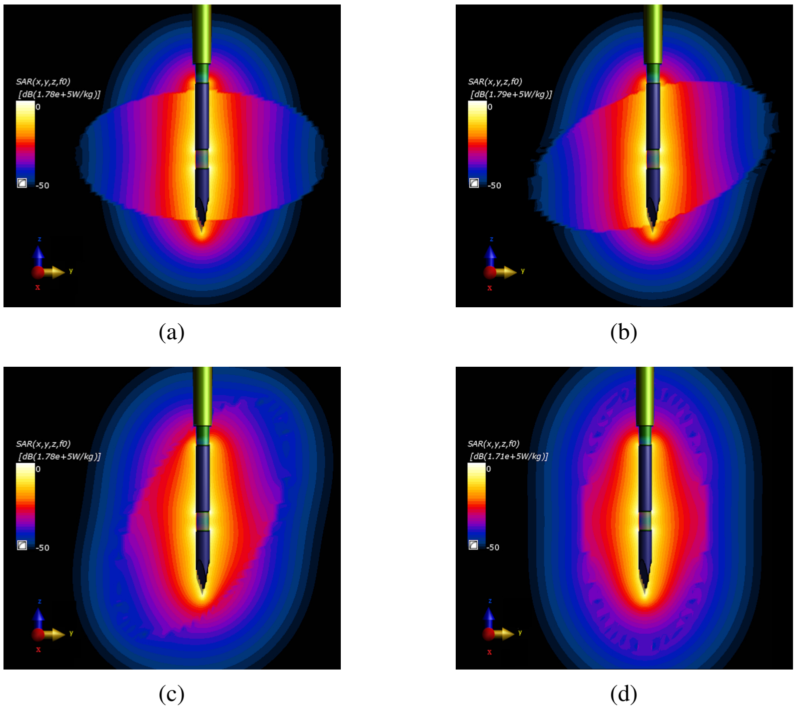

Fig. 8. SAR distributions inside liver tumor tissue in the case of various RF applicator rotation angles: (a) ϕ = 0°; (b) ϕ = 30°; (c) ϕ = 60°, and (d) ϕ = 90°

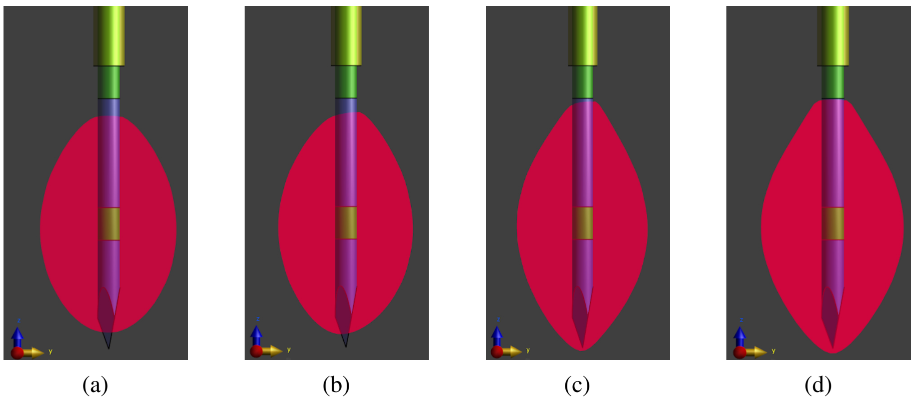

Fig. 9. The ISO-50°C surfaces inside liver tumor tissue the case of various RF applicator rotation angles: (a) ϕ = 0°; (b) ϕ = 30°; (c) ϕ = 60°, and (d) ϕ = 90°

4. Conclusions

Radiofrequency (RF) ablation is a minimally invasive technique for heating inoperable solid tumors including hepatic tissue. The type of applicator, the number of needle probes employed in thermal ablation system, the electrodes arrangement in relation to each other and their location within the targeted cancer tissue may affect the temperature level, the size and shape of the ablation zones and the shorten ablation time during hepatocellular carcinoma treatment. The proposed simulation model employed a specific voltaged needle applicator (operating at 100 kHz) inserted in the model of human liver with tumor. In our case, the irregular tumor was replaced by an equivalent ellipsoid that has the same surface and volume as the naturalistic tumor. The electro-thermal model, including the coupled Laplace equation with the modified Pennes equation, was solved using commercially available FEM-based software. The paper shows that the proposed matrix of applicators employed in single-, double- and triple-probe RF ablation system and the arrangement of electrodes generate temperature levels in the liver tumor tissue, which may play an important role in the ablation of hepatocellular carcinoma. It was observed that increasing the number of applicators causes a rise in temperature of the tumor, increases the volumes of ablation zones and improves the expected therapeutic effect of the modeled hepatic tumor. What is more, it has been proven that the rotation of the RF probe relative to the liver tumor longitudinal axis does not significantly increase the ablation zones.

References

[1] Siegel R.L., Miller K.D., Wagle N.S., Jemal A., *Cancer statistics, 2023*, CA: A Cancer Journal for Clinicians, vol. 73, no. 1, pp. 17–48 (2023), DOI: 10.3322/caac.21763.

[2] Abdalla M., Collings A.T., Dirks R. *et al.*, *Surgical approach to microwave and radiofrequency liver ablation for hepatocellular carcinoma and colorectal liver metastases less than 5 cm: A systematic review and meta-analysis*, Surgical Endoscopy, vol. 37, no. 5, pp. 3340–3353 (2023), DOI: 10.1007/s00464-022-09815-5.

[3] Miaskowski A., Gas P., *Numerical Estimation of SAR and Temperature Distributions inside Differently Shaped Female Breast Tumors during Radio-Frequency Ablation*, Materials, vol. 16, iss. 1, no. 223 (2023), DOI: 10.3390/ma16010223.

[4] Gas P., *Modelling the temperature-dependent RF ablation produced by the multi-tine electrode*, Przegląd Elektrotechniczny, vol. 96, no. 1, pp. 48–51 (2020), DOI: 10.15199/48.2020.01.12.

[5] Morega A., Morega M., Dobre A., *Hyperthermia and Ablation*, Computational Modeling in Biomedical Engineering and Medical Physics, pp. 249–294 (2021), DOI: 10.1016/B978-0-12-817897-3.00008-7.

[6] Gas P., Kurgan E., *Evaluation of thermal damage of hepatic tissue during thermotherapy based on the Arrhenius model*, 2018 Progress in Applied Electrical Engineering (PAEE), IEEE Xplore, pp. 1–4 (2018), DOI: 10.1109/PAEE.2018.8441065.

[7] Radmilovic-Radjenovic M., Boskovic N., Radjenovic B., *Computational Modeling of Microwave Tumor Ablation*, Bioengineering, vol. 9, iss. 11, no. 656 (2022), DOI: 10.3390/bioengineering9110656.

[8] Paruch M., Turchan Ł., *Mathematical modelling of the destruction degree of cancer under the influence of a RF hyperthermia*, AIP Conference Proceedings, vol. 1922, iss. 1, no. 060003 (2018), DOI: 10.1063/1.5019064.

[9] Taton G., Rok T., Rokita E., *Temperature distribution assessment during radiofrequency ablation*, 4th European Conference of the International Federation for Medical and Biological Engineering, IFMBE Proceedings, vol. 22, pp. 2672–2676 (2009), DOI: 10.1007/978-3-540-89208-3_641.

[10] Wu C., Huang H., Chen L., Yu S., Moser M.A., Zhang W., Fang Z., Zhang B., *Optimal design of aperiodic tri-slot antennas for the conformal ablation of liver tumors using an experimentally validated MWA computer model*, Computer Methods and Programs in Biomedicine, vol. 242, no. 107799 (2023), DOI: 10.1016/j.cmpb.2023.107799.

[11] Gas P., Miaskowski A., Subramanian M., *In silico study on tumor-size-dependent thermal profiles inside an anthropomorphic female breast phantom subjected to multi-dipole antenna array*, International Journal of Molecular Sciences, vol. 21, iss. 22, no. 8597 (2020), DOI: 10.3390/ijms21228597.

[12] Singla A., Marwaha A., Marwaha S., *Multi-criterion optimization of invasive antenna applicators for Au@ Fe3O4, Au@-Fe2O3 and Au@-Fe2O3 mediated microwave ablation treatment*, Electromagnetic Biology and Medicine, vol. 42, no. 1, pp. 21–40 (2023), DOI: 10.1080/15368378.2023.2184381.

[13] Avishek S., Samantaray S., *Effect of Power and Frequency on Microwave Ablation on Lungs*, 2021 8th International Conference on Signal Processing and Integrated Networks (SPIN), IEEE Xplore, pp. 26–30 (2021), DOI: 10.1109/SPIN52536.2021.9566023.

[14] Piccioni F., Poli A., Templeton L.C. *et al.*, *Anesthesia for percutaneous radiofrequency tumor ablation (PRFA): A review of current practice and techniques*, Local and Regional Anesthesia, vol. 12, pp. 127–137 (2019), DOI: 10.2147/LRA.S185765.

[15] Li J. *et al.*, *A practical pretreatment planning method of multiple puncturing for thermal ablation surgery*, Biocybernetics and Biomedical Engineering, vol. 40, no. 4, pp. 1469–1485 (2020), DOI: 10.1016/j.bbe.2020.08.004.

[16] Satish V., Repaka R., *Microwave Ablation Trocar Operated at Dual Tine Dual-Frequency: A Numerical Analysis*, Journal of Engineering and Science in Medical Diagnostics and Therapy, vol. 6, iss. 2, no. 021002 (2023), DOI: 10.1115/1.4056410.

[17] Fatigate G.R., Neves R.F.C., Lobosco M., Reis R.F., *Tissue Damage Control Algorithm for Hyperthermia Based Cancer Treatments*, Lecture Notes in Computer Science, vol. 13351 pp. 514–525 (2022), DOI: 10.1007/978-3-031-08754-7_57.

[18] Wang J., Huang S., Gao H., Liu J., Zhang Y., Wu S., *Computer Simulations of Dual-Antenna Microwave Ablation and Comparison to Experimental Measurements*, Applied Sciences, vol. 13, iss. 1, no. 26 (2022), DOI: 10.3390/app13010026.

[19] Parhar D., Baum R.A., Spouge R. *et al.*, *Hepatic Hilar Nerve Block for Adjunctive Analgesia during Percutaneous Thermal Ablation of Hepatic Tumors: A Retrospective Analysis*, Journal of Vascular and Interventional Radiology, vol. 34, no. 3, pp. 370–377 (2023), DOI: 10.1016/j.jvir.2022.11.028.

[20] Gas P., *Optimization of multi-slot coaxial antennas for microwave thermotherapy based on the S11-parameter analysis*, Biocybernetics and biomedical engineering, vol. 37, no. 1, pp. 78–93 (2017), DOI: 10.1016/j.bbe.2016.10.001.

[21] Kernot D., Yang J., Williams N., Thomas T., Ledger P., Arora H., van Loon R., *Transient changes during microwave ablation simulation: A comparative shape analysis*, Biomechanics and Modeling in Mechanobiology, vol. 22, no. 1, pp. 271–280 (2023), DOI: 10.1007/s10237-022-01646-6.

[22] Xu Y., Moser M.A., Zhang E., Zhang W., Zhang B., *Large and round ablation zones with microwave ablation: A preliminary study of an optimal aperiodic tri-slot coaxial antenna with the* π*-matching network section*, International Journal of Thermal Sciences, vol. 140, pp. 539–548 (2019), DOI: 10.1016/j.ijthermalsci.2019.03.022.

[23] Avishek S., Samantaray S., *A study on the selection of electrode materials for hepatic radiofrequency ablation: A numerical approach*, Materials Today: Proceedings, vol. 74, pp. 974–979 (2023), DOI: 10.1016/j.matpr.2022.11.348.

[24] Tang Y., Zou J., Flesch R.C., Jin T., *Effect of bio-tissue deformation behavior due to intratumoral injection on magnetic hyperthermia*, Chinese Physics B, vol. 32, iss. 3, no. 034304 (2023), DOI: 1088/1674-1056/ac744c.

[25] Tang Y., Su H., Flesch R.C., Jin T., *An optimization method for magnetic hyperthermia considering Nelder–Mead algorithm*, Journal of Magnetism and Magnetic Materials, vol. 545, no. 168730 (2022), DOI: 10.1016/j.jmmm.2021.168730.

[26] Biswas C., Nasrin R., Ahmad M.S., *Numerical analogy of bioheat transfer and microwave cancer therapy for liver tissue*, Heat Transfer, vol. 51, no. 7, pp. 6403–6430 (2022), DOI: 10.1002/htj.22597.

[27] Chaichanyut W., Chaichanyut M., *Finite Element Analysis on Porous Media: Geometric Monopole Antenna Shapes Affect Liver Tumor Microwave Ablation*, Proceedings of the 5th International Conference on Medical and Health Informatics, pp. 73–77 (2021), DOI: 10.1145/3472813.3472827.

[28] Nantivatana P., Phasukkit P., Tungjitkusolmun S., Chayakulkheeree K., *Optimal antenna slot design for hepatocellular carcinoma microwave ablation using multi-objective fuzzy decision making*, International Journal of Intelligent Engineering and Systems, vol. 13, no. 5, pp. 38–50 (2020), DOI: 10.22266/ijies2020.1031.05.

[29] Perez J.I.L., Varon L.A.B., *Estimating the Electrical Conductivity of Human Tissue in Radiofrequency Hyperthermia Therapy*, Ingenieria e Investigacion, vol. 43, no. 1, e92288 (2023), DOI: 10.15446/ing.investig.92288.

[30] Lopez J.I., Bermeo L.A., *Parametric study of thermal damage in the hyperthermia treatment by radiofrequency*, 2021 IEEE 2nd International Congress of Biomedical Engineering and Bioengineering (CI-IB&BI), IEEE Xplore, pp. 1–4 (2021), DOI: 10.1109/CI-IBBI54220.2021.9626117.

[31] Ferreira L.F.S., Bermeo Varon L.A., Orlande H.R.B., Lamien B., *Design Under Uncertainties of the Thermal Ablation Treatment of Skin Cancer*, ASME Journal of Heat and Mass Transfer, vol. 145, iss. 3, no. 031202 (2023), DOI: 10.1115/1.4055821.

[32] Kalogeropoulos A., Tsitsas N.L., *Electromagnetic interactions of dipole distributions with a stratified medium: power fluxes and scattering cross sections*, Studies in Applied Mathematics, vol. 148, no. 3, pp. 1040–1068 (2022), DOI: 10.1111/sapm.12469.

[33] Szczech M., *Experimental study on the leak mechanism of the ferrofluid seal in a water environment*, IEEE Transactions on Magnetics, vol. 57, no. 9, pp. 1–10 (2021), DOI: 10.1109/TMAG.2021.3096210.

[34] Yang C.Q., Lu M., *Safety evaluation for a high signal operator with electric field exposure induced by contact wires*, Archives of Electrical Engineering, vol. 70, no. 2, pp. 431–444 (2021), DOI: 10.24425/aee.2021.136994.

[35] Wahyudi S., Vardiansyah N.R., Setyorini P.H., *Effect of Blood Perfusion on Temperature Distribution in the Multilayer of the Human Body with Interstitial Hyperthermia Treatment for Tumour Therapy*, CFD Letters, vol. 14, no. 6, pp. 102–114 (2022), DOI: 10.37934/cfdl.14.6.102114.

[36] Garcia E.P., Rubio M.F.J.C., Lopez G.D.G., Felix K.S., Jaquez J.I.H., Chavez S.I.V., Garcia F.F., *In Silico Coaxial Antenna Design Applicator Optimization for Microwave Ablation Therapy in Medium Adipose Tissue Density Breast with Ductal Carcinoma In-Situ*, IFMBE Proceedings, vol. 96, pp. 41–49 (2024), DOI: 10.1007/978-3-031-46933-6_5.

[37] Suleman M., Riaz S., *Computational modeling of poroelastic brain tumor therapy during heat transfer carrying temperature-dependent blood perfusion*, Medical Engineering & Physics, vol. 103, no. 103792 (2022), DOI: 10.1016/j.medengphy.2022.103792.

[38] Vineeth A.J., Ramaswamy A., Ramamurthy S., *SAR analysis of radiations from a three element dipole array antenna on spherical muscle tissue in comparison with two element dipole array antenna*, AIP Conference Proceedings, vol. 2822, no. 020170 (2023), DOI: 10.1063/5.0179848.

[39] Serrano-Díaz D.G., Gomez-Flores W., Vera A., Leija L., *Towards Breast Cancer Treatment Planning by Microwave Ablation via Tumor Characterization Using Medoid-based Eigenvectors*, 2023 20th International Conference on Electrical Engineering, Computing Science and Automatic Control (CCE), IEEE Xplore, pp. 1–6 (2023), DOI: 10.1109/CCE60043.2023.10332822.

[40] Karthik V.U., Hoole S.R.H., *Hyperthermia Treatment Planning Using Shape Optimization*, 2023 International Conference on Electromagnetics in Advanced Applications (ICEAA), IEEE Xplore, pp. 32–36 (2023), DOI: 10.1109/ICEAA57318.2023.10297626.

[41] Lobato F.S., Alamy Filho J.E., Libotte G.B., Platt G.M., *Optimizing Breast Cancer Treatment Using Hyperthermia: a Single and Multi-Objective Optimal Control Approach*, Applied Mathematical Modelling, vol. 127, pp. 96–118 (2024), DOI: 10.1016/j.apm.2023.11.022.

[42] Pennes H.H., *Analysis of Tissue and Arterial Blood Temperatures in the Resting Human Forearm*, Journal of Applied Physiology, vol. 85, no. 1, pp. 5–34 (1998), DOI: 10.1152/jappl.1998.85.1.5.

[43] Michalowska J., Wac-Wlodarczyk A., Koziel J., *Monitoring of the specific absorption rate in terms of electromagnetic hazards*, Journal of Ecological Engineering, vol. 21, no. 1, pp. 224–230 (2020), DOI: 12911/22998993/112878.

[44] Hasgall P.A., Di Gennaro F., Baumgartner C., Neufeld E., Lloyd B., Gosselin M.C., Payne D., Klingenbock A., Kuster N., *IT'IS Database for Thermal and Electromagnetic Parameters of Biological Tissues*, Version 4.1 (2022), DOI: 10.13099/VIP21000-04-1.

[45] *Sim4Life Manual*, version 6.2, Zurich MedTech AG, Zurich, Switzerland (2021).